Prepared for submission to JINST

4TH European Conference on Plasma Diagnostics 2021
7TH - 11TH June 2021
Centro de Laséres Pulsados (CLPU), Salamanca, Spain

Comparison of Unfolding Methods for the Inference of Runaway Electron Energy Distribution from γ-ray Spectroscopic Measurements

E. Panontin,[a,1] **A. Dal Molin,**[b] **M. Nocente,**[a,b] **G. Croci,**[a,b] **J. Eriksson,**[c] **L. Giacomelli,**[b] **G. Gorini,**[a,b] **M. Iliasova,**[d] **E. Khilkevitch,**[d] **A. Muraro,**[b] **D. Rigamonti,**[b] **M. Salewski,**[e] **J. Scionti,**[b] **A. Shevelev,**[d] **M. Tardocchi,**[a,b] **the Eurofusion MST1 Team**[3] **and the ASDEX Upgrade Team**[4]

[a] *Dipartimento di Fisica "G. Occhialini", Università degli Studi di Milano-Bicocca, 20126 Milano, Italy*
[b] *Istituto per la Scienza e Tecnologia dei Plasmi, Consiglio Nazionale delle Ricerche, 20126 Milano, Italy*
[c] *Department of Physics and Astronomy, Uppsala University, Regementsvägen 1, SE-752 37 Uppsala, Sweden*
[d] *Ioffe Institute, 26 Politekhnicheskaya, St Petersburg 194021, Russian Federation*
[e] *Department of Physics, Technical University of Denmark, DK-2800 Kgs. Lyngby, Denmark*

E-mail: e.panontin@campus.unimib.it

Abstract: Unfolding techniques are employed to reconstruct the 1D energy distribution of runaway electrons from Bremsstrahlung hard X-ray spectrum emitted during plasma disruptions in tokamaks. Here we compare four inversion methods: truncated singular value decomposition, which is a linear algebra technique, maximum likelihood expectation maximization, which is an iterative method, and Tikhonov regularization applied to χ^2 and Poisson statistics, which are two minimization approaches. The reconstruction fidelity and the capability of estimating cumulative statistics, such as the mean and maximum energy, have been assessed on both synthetic and experimental spectra. The effect of measurements limitations, such as the low energy cut and few number of counts, on the final reconstruction has also been studied. We find that the iterative method performs best as it better describes the statistics of the experimental data and is more robust to noise in the recorded spectrum.

Keywords: Analysis and statistical methods, Nuclear instruments and methods for hot plasma diagnostics, Plasma diagnostics - charged-particle spectroscopy, Plasma diagnostics - interferometry, spectroscopy and imaging, Detector modelling and simulations I, Radiation-hard detectors, Gamma detectors

[1] Corresponding author.
[2] See author list of B. Labit et al. 2019 Nucl. Fusion 59 086020
[3] See author list of H. Meyer et al. 2019 Nucl. Fusion 59 112014

Contents

1 Introduction **1**

2 Analysis techniques **1**

3 Synthetic tests **2**

4 Application to AUG data **3**

5 Conclusions **5**

1 Introduction

In recent years, the development of a new generation of hard-X ray (HXR) spectrometers, based on $LaBr_3$ inorganic scintillators with counting rates capabilities up to 1 MCps and energy resolution of $\lesssim$ 5 % @ 661 keV [1, 2], allowed to measure the Bremsstrahlung radiation emitted from the interaction between runaway electrons (REs) and background ions during plasma disruptions in tokamaks [3]. From this HXR spectrum, the 1D energy distribution of the beam can be reconstructed using suitable unfolding techniques [4, 5], unveiling precious information for the study of REs dynamics and the design of avoidance or mitigation strategies for ITER. In addition to being computationally less expensive, measured 1D energy distribution functions can challenge computations from first principles to improve our understanding of REs.

The performance of unfolding techniques strongly depends on the process under analysis, thus the comparison of different deconvolution methods on synthetic distributions can help assessing the capability and limits of the unfolding procedure. In this work we present a comparison of four unfolding techniques, which are presented in section 2 and then applied to synthetic signals (section 3) as well as to experimental data collected with the 1"x1" cylindrical $LaBr_3$ scintillator installed in the Bragg Bunker at ASDEX Upgrade (AUG) (section 4).

2 Analysis techniques

The HXR spectrum $\underline{S}$ and the RE energy distribution $\underline{F}$ follow the convolution equation: $\underline{S} = \underline{\underline{W}} \cdot \underline{F}$, which is the same method as applied in energetic ion distribution functions [6]. Here the matrix $\underline{\underline{W}}$ describes the Bremsstrahlung emission probability, which was calculated using the GENESIS code [7], and the interaction of a photon with a $LaBr_3$ scintillator, which was simulated using the MCNP code [8]. Figure 1 shows a sketch of $\underline{\underline{W}}$'s columns, which represent the spectra emitted by a ideally mono-energetic RE beam, and rows, which are also called weight functions [19, 20] and describe the diagnostic sensitivity to different regions in the RE energy spectrum. In this section we present four unfolding techniques, whose performances on the problem at hand will be compared in sections 3 and 4.

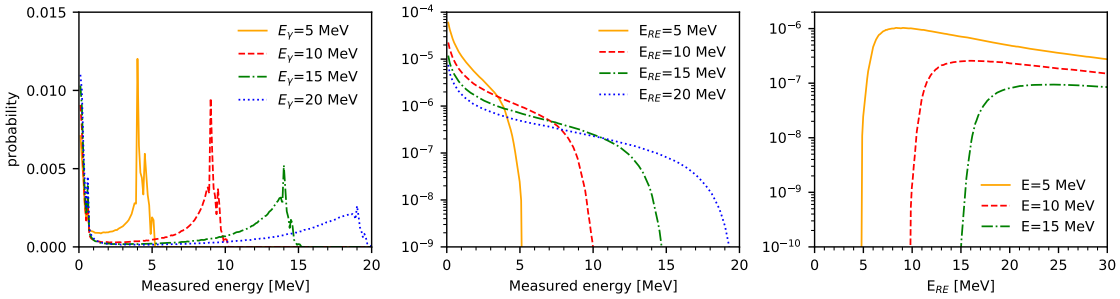

Figure 1. (left) MCNP simulation of the DRF of the $LaBr_3$ scintillator installed at AUG in the Bragg Bunker. Transfer matrix $\underline{\underline{W}}$ columns (centre) and rows (right), the latter for 5, 10 and 15 MeV measured signals.

Singular Value Decomposition (SVD) [9] is a linear algebra method for the spectral decomposition of a rectangular matrix into orthogonal matrices, which in turn can be transposed to give the truncated pseudo inverse: $\underline{\underline{W}}^{-1} = \underline{\underline{V}} \cdot \underline{\underline{\Sigma}}^{-1} \cdot \underline{\underline{U}}^T$. Here $\underline{\underline{U}}$ and $\underline{\underline{V}}$ are the singular vectors matrices, while $\underline{\underline{\Sigma}}$ is the diagonal matrix containing $\underline{\underline{W}}$ singular values. In order to smooth any computational and experimental noise that might degrade the reconstruction $\underline{\underline{\Sigma}}$ is usually truncated by neglecting all singular values smaller than a custom threshold. Maximum Likelihood - Expectation Maximization (ML-EM) is an iterative algorithm commonly used in tomographic inversions [4, 10]: it makes a first guess (e.g. $F_i^0 = \sum_j \frac{W_{ji}}{\sum_i W_{ji}} S_j$) and evolves according to: $F_i^{n+1} = F_i^n \sum_j \frac{W_{ij}}{\sum_l W_{li}} \frac{S_j}{\sum_k W_{jk} F_k^n}$, n being the iteration number. Every $n_{smoothing}$ iteration the estimate is smoothed by applying a sliding window average filter to prevent the formation of artifacts. Tikhonov regularization traditionally minimizes the χ^2 statistics and a smoothing operator $\underline{\underline{L}}$ [11–16], that in the present work has been chosen of the first order (i.e. it penalizes steep gradients in the reconstruction). The solution, then, is chosen as: $\underline{F} = \arg\min_{\underline{F} \geq \underline{0}} \left(\|\underline{\underline{W}} \cdot \underline{F} - \underline{S}\|^2 + \alpha \|\underline{\underline{L}} \cdot \underline{F}\|^2 \right)$, where the parameter $\alpha \geq 0$ determines the intensity of the smoothing. Finally, we have also tested a variation of Tikhonov regularization, where the χ^2 has been substituted by the Poisson log-likelihood calculated in ref. [17]: $\ell = \sum_i \left(\left[\underline{\underline{W}} \cdot \underline{F} \right]_i + \beta \right) - \sum_i \left(S_i \log(\left[\underline{\underline{W}} \cdot \underline{F} \right]_i + \beta) \right)$, which better describes our data. Here β is a small arbitrary parameter that prevents the cost function from diverging.

In all four methods the smoothing parameters have been set according to the L-curve method, as in ref. [11], while the confidence band of the reconstruction has been computed with the Monte Carlo procedure proposed in ref. [18]. Since each of the methods presented suffers from the generation of artifacts in the reconstructed distribution, cumulative statistics has been studied as well. In particular the RE mean energy and the maximum energy, calculated as the X percentile of the energy distribution, with X = 90 % and 99 %. and 99.9 %.

3 Synthetic tests

The performance of the methods explained in section 2 have been tested on four synthetic RE energy distributions (figure 2): a gaussian (μ = 12 MeV, σ = 3 MeV), an exponential (τ = 10 a.u.), a maxwellian (τ = 40 a.u.) and the sum of a maxwellian and a gaussian (τ = 40 a.u., μ = 12 MeV, σ = 1 MeV). SVD shows severe artifacts in most reconstructionss: negative probability functions

Table 1. Mean energy and maximum energy (calculated as the 90, 99, 99.9 percentiles) of the synthetic distribution function shown in figure 2 reconstructed with the four methods presented in section 2. The errors are estimated using a Monte Carlo procedure on the reconstructed RE distribution.

gaussian [MeV]	SVD [MeV]	ML-EM [MeV]	Tikhonov [MeV]	Poisson [MeV]
$\langle E \rangle = 12.00$	11.80 ± 0.10	12.01 ± 0.12	12.18 ± 0.3	11.95 ± 0.4
$E^{90} = 15.76$	15.15 ± 0.10	15.8 ± 0.1	16.47 ± 0.5	15.97 ± 0.5
$E^{99} = 18.91$	16.58 ± 2	18.91 ± 1.7	19.22 ± 1.5	18.10 ± 1.3
$E^{99.9} = 21.25$	25.83 ± 0.3	21.66 ± 5	20.24 ± 1.3	19.02 ± 1.2
exponential	SVD	ML-EM	Tikhonov	Poisson
$\langle E \rangle = 8.48$	8.55 ± 0.06	8.54 ± 0.09	8.79 ± 0.19	8.53 ± 0.4
$E^{90} = 19.32$	20.03 ± 0.3	19.22 ± 0.4	20.34 ± 1.1	19.22 ± 1.6
$E^{99} = 28.27$	28.68 ± 0.5	28.47 ± 0.9	28.88 ± 1.4	28.58 ± 2
$E^{99.9} = 29.80$	29.90 ± 0.4	29.90 ± 0.5	29.90 ± 0.9	29.90 ± 1.8
maxwellian	SVD	ML-EM	Tikhonov	Poisson
$\langle E \rangle = 7.14$	7.04 ± 0.07	7.18 ± 0.06	7.05 ± 0.02	7.10 ± 0.5
$E^{90} = 11.08$	10.78 ± 0.10	11.19 ± 0.15	10.88 ± 0.1	10.98 ± 1.0
$E^{99} = 15.05$	14.13 ± 7	15.46 ± 1.1	13.63 ± 0.2	14.13 ± 2.0
$E^{99.9} = 18.00$	22.78 ± 2	19.22 ± 7	15.05 ± 1.0	15.25 ± 1.9
maxwellian+gaussian	SVD	ML-EM	Tikhonov	Poisson
$\langle E \rangle = 6.25$	6.06 ± 0.11	6.18 ± 0.12	6.11 ± 0.08	6.18 ± 0.6
$E^{90} = 10.98$	10.47 ± 0.4	10.88 ± 0.4	10.58 ± 0.2	10.88 ± 2
$E^{99} = 14.13$	13.32 ± 5	13.63 ± 4	13.32 ± 0.9	13.52 ± 1.7
$E^{99.9} = 15.35$	13.73 ± 6	14.74 ± 4	14.34 ± 0.9	14.24 ± 1.6

and evident oscillations around 0 at high and low energy. The other three methods give better results, eventhough traditional Tikhonov regularization often underestimates the high-energy tail of the distribution. Table 1 reports the estimates of the mean energy of the RE beam ($\langle E \rangle$) and its maximum energy, as defined in section 2. The errors (σ) of the estimates have been computed using the Monte Carlo procedure of ref. [18]. The worst results are again obtained using SVD, which will not be included in the analysis of section 4. The best results are obtained using ML-EM: the estimates always differ from the true statistics less of ≈ 5 % and the Monte Carlo error always accounts for this difference within one σ.

4 Application to AUG data

The reconstructions of AUG shot #34084 (see also ref. [3]), obtained using the unfolding methods presented in section 2, are compared in figure 3. All methods retrieve admissible solutions, which well fit the experimental data. The reconstructed RE energy distributions are in good agreement up to ≈ 10 MeV, while they differ in the high-energy tail. As already pointed out in section 3, Tikhonov regularization with χ^2 statistics is prone to underestimate such a tail.

A cut at low energy between 0.1 and 0.5 MeV is always applied to the measured spectra in order to remove the electronic noise due to the acquisition chain. To determine the effect of this loss

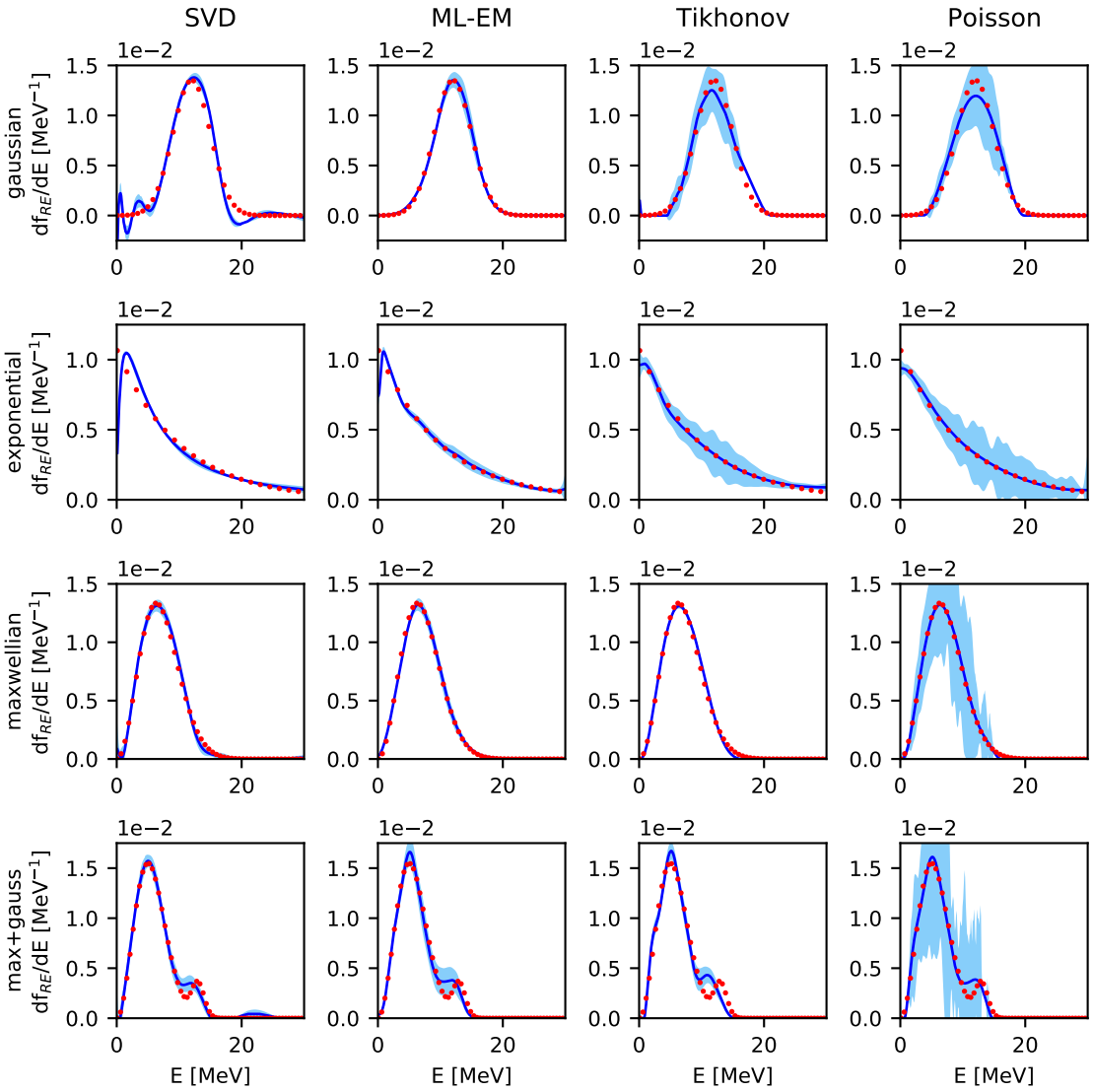

Figure 2. Reconstructions of four synthetic signals: a gaussian, an exponential, a maxwellian and the superposition of a maxwellian with a gaussian. The RE distribution used to generate the synthetic signal is reported in red dots, while its reconstruction is shown as a blue line with statistical errors shown as a light-blue band.

of information on the final reconstruction, shot #34084 has been analysed after applying different energy cuts from 0.1 to 6 MeV (figure 4). Some minor artifacts appear in a region of $\approx 2-3$ MeV right above the cut and the peaks in the high energy part of the distribution are accentuated. However the overall spectral shape of the reconstruction is preserved, showing that the low energy cut determines mainly the reconstruction below ≈ 5 MeV, while the shape of the high-energy part of the RE energy distribution is mostly influenced by the high-energy counts in the HXR spectrum.

We are also interested in studying the minimum number of counts necessary to perform a

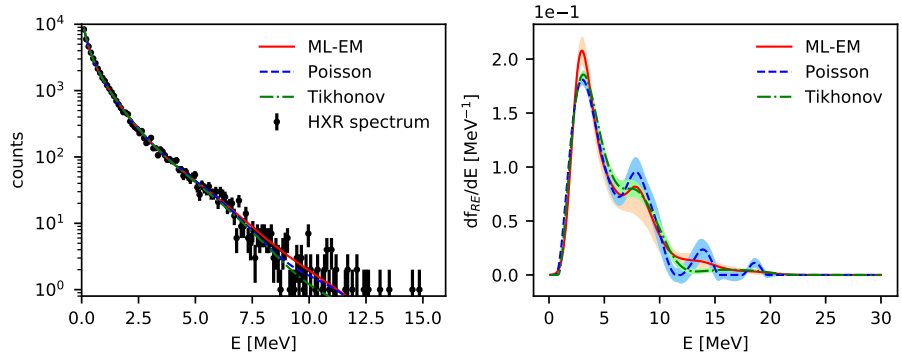

Figure 3. (left) The experimental HXR spectrum measured during AUG shot #34084 in the time interval 1.00 - 1.13 s and its reconstruction obtained convolving the RE distributions (see graph on the right) with the transfer matrix W (see figure 1). (right) REs energy distribution reconstructed from the experimental spectrum shown on the left, using ML-EM, Poisson and Tikhonov regularizations.

reconstruction of the RE energy distribution. Statistically independent, uniformly drawn, random samples of the shot #34084 HXR spectrum, with 1, 5, 10 and 20 kcounts have been analysed. The reconstructions performed with Tikhonov minimization applied to the Poissonian statistics show substantial differences already when 20 kcounts draws are analysed, thus suggesting that the signal to noise ratio of the high-energy tail of the RE Bremsstrahlung emission is unfavorable for the Poissonian cost function and that the two peaks above 10 MeV in figure 3 are probably an artefacts. Better results are achieved using ML-EM and traditional Tikhonov regularization, which can retrieve the overall shape of RE energy distribution even with only 5/10 kcounts. When only global features of the RE beam are seeked, the above recommendation can be relaxed: figure 4 shows the average and standard deviation of $\langle E_{RE} \rangle$, E_{RE}^{90} and E_{RE}^{99} calculated on multiple draws. The inference of the mean RE energy gives good results also on spectra with only 1 kcounts, while the estimates for the maximum energy are reliable on average up to 5 kcounts (the higher the percentile of the estimate, the more counts are needed).

5 Conclusions

Four unfolding techniques have been applied to the reconstruction of the runaway electrons energy distribution from their Bremsstrahlung HXR emission. ML-EM has produced the most reliable reconstruction of the synthetic signals. With all four methods, the mean and maximum energy of the RE beam has been estimated within 5% from the true value, proving those estimates to be robust against the presence of artifacts in the reconstruction. The tests performed on experimental data show that ML-EM and Tikhonov with χ^2 statistics give good results also when a generous low-energy cut is applied. The two methods also perform well with limited statistics, reaching a maximum time resolution of $\approx 10^{-2}$ s if the complete spectral information is required, which can be pushed to $\approx 10^{-3}$ s for the estimate of the cumulative statistics.

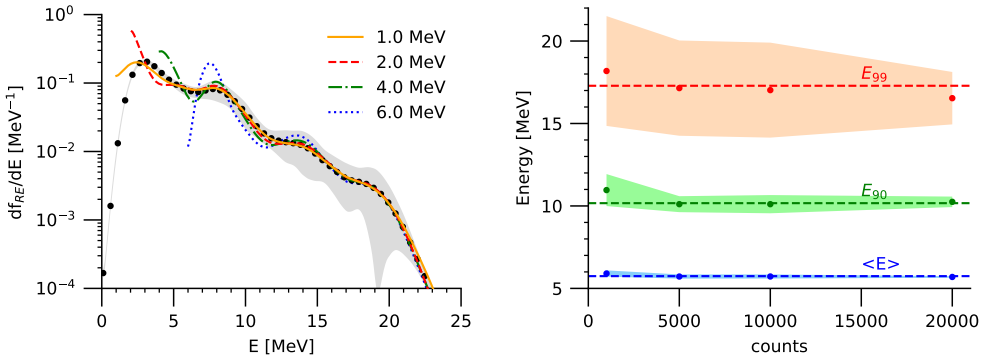

Figure 4. (left) Multiple reconstructions of the RE energy distribution in AUG shot #34084 for different low energy cuts, performed with ML-EM. Black dots show the reconstruction of figure 3 for reference. (right) Average and standard deviation of RE distribution statistics obtained by reconstructing random draws of the experimental data set, with variable size (1, 5, 10, 20 kcounts), using ML-EM. Dashed lines refer to the statistics of the reconstruction in figure 3

Acknowledgments

This work has been carried out within the framework of the EUROfusion Consortium and has received funding from the Euratom research and training programme 2014-2018 and 2019-2020 under grant agreement No 633053. The views and opinions expressed herein do not necessarily reflect those of the European Commission.

References

[1] D. Rigamonti et al, *The upgraded JET gamma-ray cameras based on high resolution/high count rate compact spectrometers*, *Rev. Sci. Instrum.* **89** (2018) 10I116

[2] M. Nocente et al, *Gamma-ray spectroscopy at MHz counting rates with a compact LaBr3 detector and silicon photomultipliers for fusion plasma applications*, *Rev. Sci. Instrum.* **87** (2016) 11E714

[3] M. Nocente et al, *High resolution gamma-ray spectrometer with MHz capabilities for runaway electron studies at ASDEX Upgrade* , *Rev. Sci. Instrum.* **89** (2018) 10I124

[4] A.E. Shevelev et al, *Reconstruction of distribution functions of fast ions and runaway electrons in fusion plasmas using gamma-ray spectrometry with applications to ITER*, *Nucl. Fusion* **53** (2013) 123004

[5] A. Dal Molin *PhD thesis* (2021) https://boa.unimib.it/handle/10281/304289

[6] M. Salewski et al, *Combination of fast-ion diagnostics in velocity-space tomographies*, *Nucl. Fusion*, **53** (2013) 063019

[7] M. Nocente et al, *Conceptual design of the radial gamma ray spectrometers system for α particle and runaway electron measurements at ITER*, *Nucl. Fusion* **57** (2017) 076016

[8] T. Goorley et al., *Initial MCNP6 Release Overview*, *Nuclear Technology* 180 (2012) 298-315

[9] D. Kalman, *A Singularly Valuable Decomposition: The SVD of a Matrix Coll. Math* **27** (1996) 2-23

[10] E. Panontin et al, *First spatially resolved measurements of the D–^{3}He α-particle source with the upgraded JET gamma-ray camera*, *Rev. Sci. Instrum.* **92** (2021) 053529

[11] A. S. Jacobsen et al, *Inversion methods for fast-ion velocity-space tomography in fusion plasmas*, *Plasma Phys. Control. Fusion* **58** (2016) 045016

[12] B Madsen et al, *Fast-ion velocity-space tomography using slowing-down regularization in EAST plasmas with co- and counter-current neutral beam injection Plasma Phys. Control. Fusion* **62** (2020) 115019

[13] B. Madsen et al, *Tomography of the positive-pitch fast-ion velocity distribution in DIII-D plasmas with Alfvén eigenmodes and neoclassical tearing modes*, *Nucl. Fusion* **60** (2020) 066024

[14] M Weiland et al, *Enhancement of the FIDA diagnostic at ASDEX Upgrade for velocity space tomography*, *Plasma Phys. Control. Fusion* **58** (2016) 025012

[15] M Weiland et al, *Phase-space resolved measurement of 2nd harmonic ion cyclotron heating using FIDA tomography at the ASDEX Upgrade tokamak*, *Nucl. Fusion* **57** (2017) 116058

[16] M Salewski et al, *High-definition velocity-space tomography of fast-ion dynamics*, *Nucl. Fusion* **56** (2016) 106024

[17] J. M. Bardsley and N. Laobeul, *Tikhonov regularized Poisson likelihood estimation: theoretical justification and a computational method*, *Inverse Probl. Sci. Eng.* **16.2** (2008) 199–215

[18] D. G. Shirk and N. M. Hoffman, *Monte-Carlo error analysis in x-ray spectral deconvolution Rev. Sci. Instrum.* **56** (1985) 809

[19] M Salewski et al, *Fast-ion energy resolution by one-step reaction gamma-ray spectrometry*, *Nucl. Fusion* **56** (2016) 046009

[20] M Salewski et al, *Velocity-space observation regions of high-resolution two-step reaction gamma-ray spectroscopy*, *Nucl. Fusion* **55** (2015) 093029